Periodic mesoporous organogold(I)silica as an active and reusable catalyst for alkyne hydration

Fengxia Zhu, Fang Zhang, Xushi Yang, Jianlin Huang, Hexing Li*

The Education Ministry Key Lab. of Res. Chem., Shanghai Normal University, Shanghai 200234, PR China

ABSTRACT

A periodic mesoporous organogold(I)silica catalyst was synthesized by surfactant-directed co-condensation of Au[PPh$_2$(CH$_2$)$_2$Si(OCH$_2$CH$_3$)$_3$]$_2$Cl and (CH$_3$CH$_2$O)$_3$SiPhSi(OCH$_2$CH$_3$)$_3$. The as-prepared Au–PPh$_2$–PMO(Ph) contained ordered mesopore channels with both phenyl (Ph) group and Au(I) organometal homogeneously embedded in silica walls. Such catalyst exhibited higher activity than free Au(PPh$_3$)Cl in hydration reactions of various terminal alkynes. This could be mainly attributed to the high surface area, the ordered mesoporous channels and the enhanced surface hydrophobility, which facilitated the diffusion and adsorption of reactants. Meanwhile, the unique coordination model between Au(I) and (PPh$_2$) was also favorable for the alkyne hydration. Besides the high activity, the catalyst could be easily recycled and used repetitively owing to the high hydrothermal stability and the stabilized Au(I) active sites against leaching.

1. Introduction

Organometallic catalysts have been widely used in organic synthesis owing to the high activity and selectivity [1,2]. However, it was limited in practical application because of the complicated separation procedures from the reaction mixture as well as the difficulties in recycling, which will inevitably lead to high cost and even environmental pollutions from heavy metallic ion [3,4]. Heterogeneous catalysts could overcome these limitations, but they usually displayed poor catalytic activity and selectivity [5–8] due to the low dispersion of active sites, the enhanced diffusion limit, and the change of chemical microenvironment of active sites. Mesoporous silica supports with high surface and ordered mesopore channels allow to prepare immobilized organometallic catalysts with high dispersion and low diffusion limit [9,10]. Meanwhile, the functionalization with organic groups could enhance the surface hydrophobicity which may facilitate the diffusion and adsorption of organic reactant molecules, especially in aqueous medium [11]. However, the organometals and organic functionalities terminally bonded to the pore surface might partially block the pore channels, which might disfavor the catalytic efficiency. Moreover, they would easily suffer from leaching during liquid phase reactions, leading to the poor durability [12–14].

Periodic mesoporous organosilicas (PMO) with organic groups (e.g. methyl, ethyl, phenyl, biphenyl and amine) homogeneously embedded in silica walls could diminish the pore blockage and also inhibit the leaching of organic functionalities [15–19]. Previously, we developed a general strategy to design periodic mesoporous organometalsilica catalysts with organometals and organic groups as the integral part of the pore walls [12,13]. Herein, as the continueved research studies of powerful immobilized catalysts, we report the synthesis of a periodic mesoporous organogold(I)silica catalyst with both Au(I) organometals and phenyl groups (Ph) integrally incorporating into silica framework. Its catalytic performance was evaluated in hydration reactions of various terminal alkynes, which showed both high activity and strong durabilty comparing to the similar catalyst with Au(I) organometals terminally bonded to the Ph-bridged PMO support or even the Au(PPh$_3$)Cl homogeneous catalyst.

2. Experimental

2.1. Catalyst preparation

Firstly, the Au[PPh$_2$(CH$_2$)$_2$Si(OCH$_2$CH$_3$)$_3$]$_2$Cl was synthesized by mixing 10 mL CH$_2$Cl$_2$, 0.064 g Au(tht)Cl (tht = tetrahydrothiophene) and 0.15 mL PPh$_2$CH$_2$CH$_2$Si(OCH$_2$CH$_3$)$_3$ under argon atmosphere, followed by stirring at 25 °C for 2 h. The solid product was collected by evaporating CH$_2$Cl$_2$, followed by washing with dried petroleum ether and drying under vacuum at 25 °C for 24 h. Then, the periodic

---

* Corresponding author. Tel.: +86 21 64322272; fax: +86 21 64322272.
E-mail address: Hexing-Li@shnu.edu.cn (H. Li).
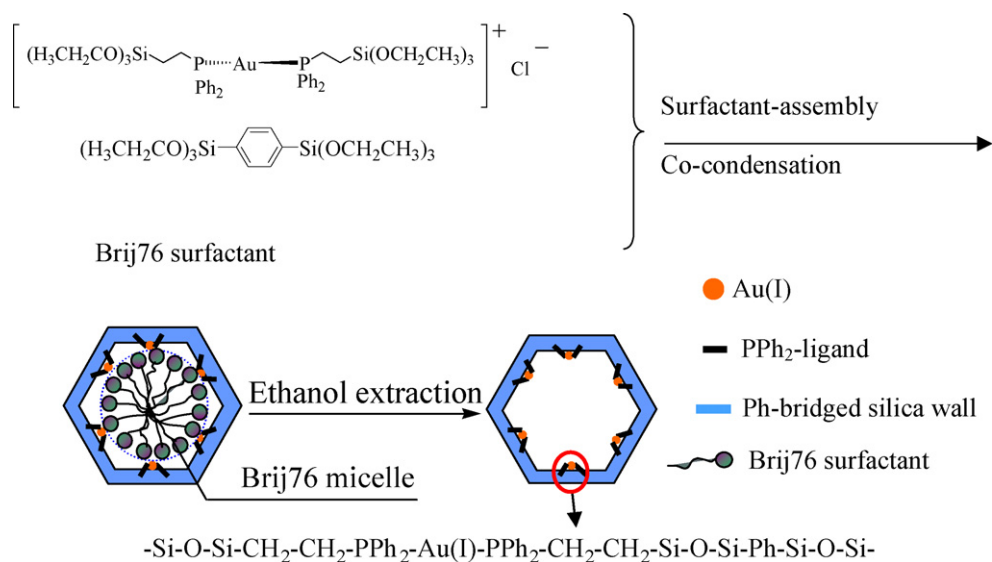
Scheme 1. Illustration of preparing Au–PPh$_2$–PMO(Ph).

mesoporous organogold(I)silica, denoted as Au–PPh$_2$–PMO(Ph), was prepared according to the procedures illustrated in Scheme 1. In a typical run of synthesis, 1.3 mL 37% HCl aqueous solution, 0.40 g poly(oxyethylene) (10) stearyl ether (Brij 76) and 0.76 g (CH$_3$CH$_2$O)$_3$SiPhSi(OCH$_2$CH$_3$)$_3$ were mixed in 19 mL distilled H$_2$O. After being prehydrolyzed for 20 min at 50 °C, 1.0 mL tetrahydrofuran (THF) containing 0.16 g Au[PPh$_2$(CH$_2$)$_2$Si(OCH$_2$CH$_3$)$_3$]$_2$Cl was added into the solution, followed by stirring at 50 °C for 12 h and aging at 100 °C for another 24 h. The molar ratio of Si:Brij76:HCl:H$_2$O was 1.0:0.17:6.0:417, where Si referred to the total silicon source. The solid product was filtrated and dried under vacuum for 24 h. Finally, the surfactants and other organic substances were extracted and washed away by refluxing in ethanol solution at 80 °C for 24 h. The Au(I) loading was determined as 0.22 wt% by ICP analysis.

For comparison, the Au(I) organometal was also immobilized onto Ph-bridged PMO support via grafting method and denoted as Au–PPh$_2$–PMO(Ph)–G. Briefly, 0.40 g Brij 76, 1.3 mL 37% HCl, 0.76 g (CH$_3$CH$_2$O)$_3$SiPhSi(OCH$_2$CH$_3$)$_3$ and 0.070 g PPh$_2$CH$_2$CH$_2$Si(OCH$_2$CH$_3$)$_3$ were mixed in 19 mL distilled H$_2$O. After stirring for 12 h at 50 °C, the mixture was transferred into an autoclave for 24 h hydrothermal treatment at 100 °C. The solid product, denoted as PPh$_2$–PMO(Ph), was collected and extracted in ethanol solution at 80 °C for 24 h to remove Brij76 and other organic residues. Then, 1.0 g PPh$_2$–PMO(Ph) and 0.049 g Au(PPh$_3$)Cl were mixed in 10 mL toluene solution and stirred for 24 h at room temperature. The solid product was dried at 80 °C under vacuum, followed by Soxlet-extraction with CH$_2$Cl$_2$ for another 24 h to remove physisorbed Au(I) species on the support. The Au(I) loading was determined as 0.26 wt% by ICP analysis.
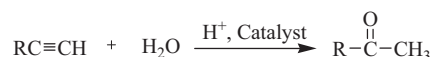
2.2. Characterization

The compositions and Au(I) loadings were determined by elemental analysis (Elementar Vario ELIII, Germany) and inductively coupled plasma optical emission spectrometer (ICP-OES, Varian VISTA-MPX). Fourier transform infrared (FTIR) spectra were collected on a Nicolet Magna 550 spectrometer by using the KBr method. Solid-state NMR spectra were recorded on a Bruker AV-400 spectrometer. Thermogravimetric analysis and differential thermal analysis (TG/DTA) were conducted on a DT-60. Low-angle X-ray powder diffraction (XRD) patterns were obtained on a Rigaku D/maxr B diffractometer with Cu Ka. N$_2$ adsorption–desorption isotherms were measured at 77 K on a Quantachrome NOVA 4000e analyzer, from which the specific surface area (S_{BET}) was calculated by applying Brunauer–Emmett–Teller (BET) method and Barrett–Joyner–Halenda (BJH) model on the adsorption branches, respectively. Meanwhile, the average pore diameter (D_P) and total pore volume (V_P) were calculated from the adsorption isotherms using Barrett–Joyner–Halenda (BJH) model. Surface morphologies and porous structures were observed through a transmission electron microscopy (TEM, JEOL JEM2011). The surface electronic states were analyzed by X-ray photoelectron spectroscopy (XPS, Perkin-Elmer PHI 5000C). All the binding energy (BE) values were calibrated by using the standard BE value of contaminant carbon ($C_{1S} = 284.6$ eV) as a reference.

2.3. Activity test

The hydration reactions of terminal alkynes (see Scheme 2) were carried out at 100 °C in a 10 mL round-bottomed flask by adding a catalyst containing 0.010 mmol Au(I), 0.25 mmol alkyne, 0.25 mmol H$_2$SO$_4$, 4.0 mL distilled water and n-decane as an internal standard. After stirring for 7 h, the products were extracted by acetic ether, followed by analysis on a gas chromatograph (SHIMADZU, GC-17A) equipped with a JWDB-5, 95% dimethyl-1-(5%)-diphenylpolysiloxane column and a FID detector. The column temperature was programmed from 80 to 250 °C at a ramp speed of 10 °C/min N$_2$ was used as carrier gas. The reproducibility was checked by repeating each result at least three times and was found to be within ±5%.

In order to determine the catalyst durability, the catalyst was allowed to centrifuge after each run of reactions and the clear supernatant liquid was decanted slowly. The catalyst was washed thoroughly with distilled water and ethanol, followed by drying at 80 °C for 8 h under vacuum condition. Then, the catalyst was reused with fresh charge of reactants for subsequent recycle under the identical reaction conditions.

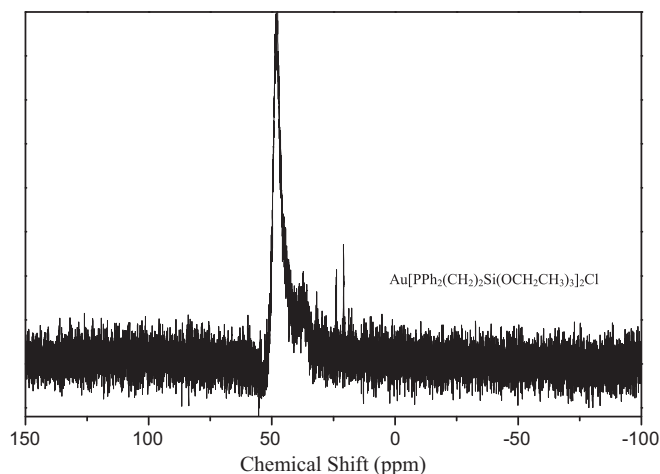**Scheme 2.** Chemical equation of the hydration reactions with terminal alkynes.

Fig. 1. ^{31}P NMR spectrum of Au[PPh$_2$(CH$_2$)$_2$Si(OCH$_2$CH$_3$)$_3$]$_2$Cl.

3. Results and discussion

3.1. Structural characteristics

The composition and chemical formula of the Au(I) organometal-brideged silane were determined as Au[PPh$_2$(CH$_2$)$_2$Si(OCH$_2$CH$_3$)$_3$]$_2$Cl based on ICP analysis (P/Au molar ratio = 2.01), elemental analysis (calculated: C 49.45, H 5.45; experimental: C 49.25, H 5.55), melting point test (125 °C), ^{1}H NMR (CDCl$_3$): δ = 7.7–7.3 (m, 20 H, Ph); 3.6 (q, 12H), 2.50 (m, 4 H, CH$_2$–P); 1.1 (t, 18H, Me); 0.60 (m, 4 H, SiCH$_2$), and ^{31}P NMR spectrum (see Fig. 1). The FTIR spectra (Fig. 2) displayed no significant signals indicative of Brij76, implying that the surfactant in Au–PPh$_2$–PMO(Ph) was mostly removed after extraction in ethanol. The Au–PPh$_2$–PMO(Ph) exhibited three absorbance bands at 1064, 1152, and 1449 cm^{-1} characteristic of the vibrations from Si–O, Si–C and P–C bonds [20,21], which were similar to those observed in Au[PPh$_2$CH$_2$Ch$_2$Si(OCH$_2$CH$_3$)$_3$]$_2$Cl, indicating the successful incorporation of Au(I) organometal into the silica framework. The other three peaks around 640, 1377 and 3050 cm^{-1} could be assigned to δ(C–H), ν(C–C) and ν(C–H) vibrations from benzene ring [22,23]. As shown in Fig. 3, the ^{29}Si MAS NMR spectrum revealed that the Au–PPh$_2$–PMO(Ph) displayed three peaks downfield corresponding to T^1 (δ = −64 ppm), T^2 (δ = −74 ppm) and T^3 (δ = −79 ppm), where T^m = RSi(OSi)$_m$–(OH)$_{3-m}$, m = 1–3. No Q^n peaks
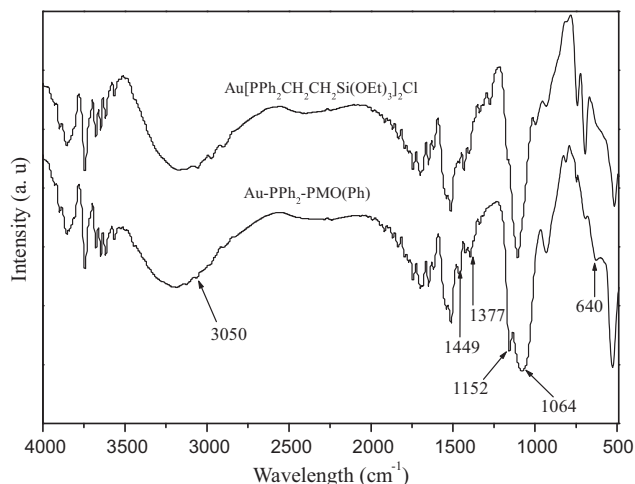
Fig. 2. FTIR spectra of the Au[PPh$_2$CH$_2$CH$_2$Si(OEt)$_3$]$_2$Cl and Au–PPh$_2$–PMO(Ph).
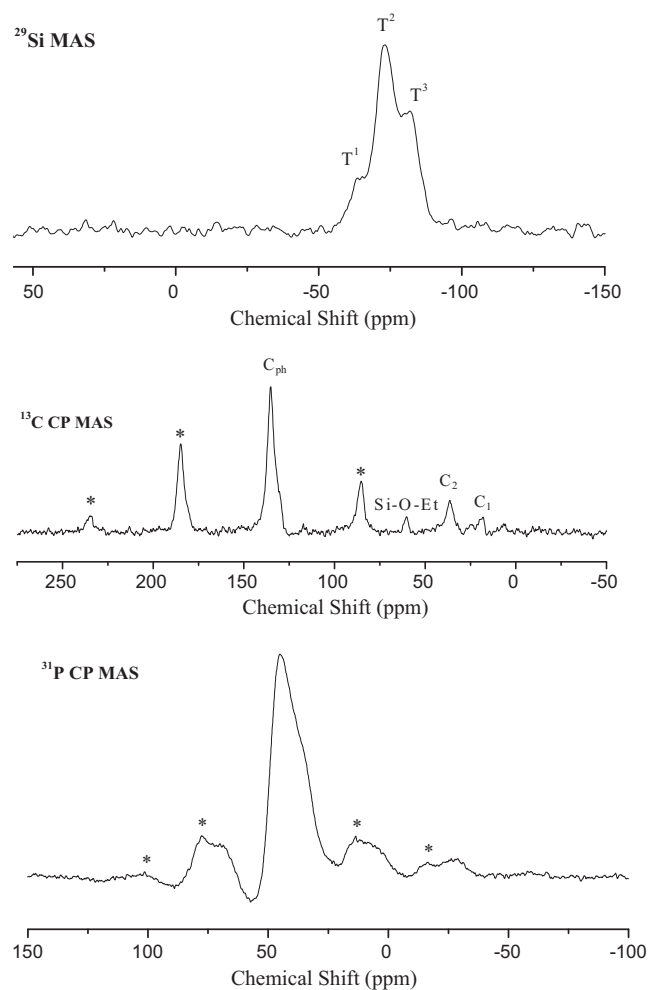
Fig. 3. Solid NMR spectra of Au–PPh$_2$–PMO(Ph).

were observed, where Q^n = Si(OSi)$_n$–(OH)$_{4-n}$, n = 2–4, indicating that all the Si species were covalently bonded with carbon atoms [24]. Meanwhile, two peaks around 18 and 38 ppm were observed in the ^{13}C CP MAS NMR spectrum, which could be assigned to two C atoms in the –CH$_2$–CH$_2$– group connecting with the PPh$_2$-group. An intense peak around 135 ppm could be attributable to the C atoms in the benzene ring (Ph). A weak peak around 59 ppm was assigned to the C atoms in the C$_2$H$_5$O-group connecting with silicon due to the incomplete hydrolysis [25]. Other peaks denoted by asterisks were ttributed to spinning sidebands, as verified by changing rotating speeds [26]. In addition, the ^{31}P CP MAS NMR spectrum revealed that the Au–PPh$_2$–PMO(Ph) displayed only one signal at 45 ppm indicative of P atom in the PPh$_2$-group, similar to that found in the Au[PPh$_2$(CH$_2$)$_2$Si(OCH$_2$CH$_3$)$_3$]$_2$Cl, indicating the unique coordination model between PPh$_2$ and Au(I). These results clearly demonstrated the presence of both the Au(I) organometal and the Ph group in the Au–PPh$_2$–PMO(Ph).

Fig. 4 shows TG/DTA curves of the Au–PPh$_2$–PMO(Ph). A weak endothermic peak around 65 °C with weight loss of about 7% could be attributed to desorption of water, CH$_2$Cl$_2$, ethanol or other organic residues. An exothermic peak around 283 °C with weight loss less than 1% could be assigned to the oxidation removal of residual C$_2$H$_5$O-groups connecting with silicon due to the incomplete hydrolysis (see the ^{13}C CP MAS NMR spectrum in Fig. 3). A broad exothermic peak ranging from 320 to 500 °C with weight loss around 7% might be responsible for the oxidation removal of –PPh$_2$–CH$_2$CH$_2$– groups bridging Au(I) and Si. An intense exother-

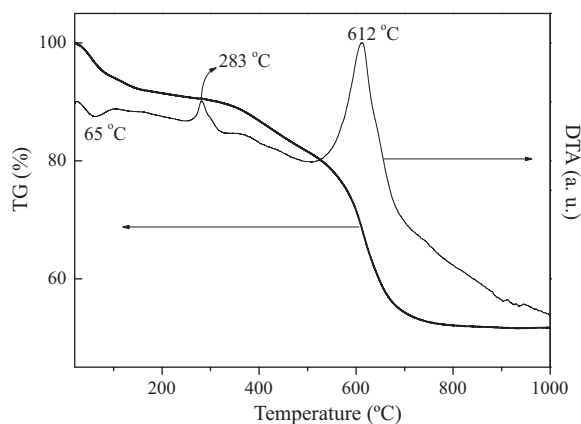**Fig. 4.** TG and DTA curves of Au–PPh$_2$–PMO(Ph).

Fig. 6. N$_2$ adsorption–desorption isotherm of Au–PPh$_2$–PMO(Ph).

mic peak at 612 °C corresponding to weight loss around 28% was resulted from the oxidation removal of phenyl groups embedded in silica walls [24,27]. The weight losses were consistent with the theoretical values, which further confirmed the presence of both the Au(I) organometals and the Ph groups in the Au–PPh$_2$–PMO(Ph).

As shown in Fig. 5, the XPS spectra demonstrated that all the Au species in the Au–PPh$_2$–PMO(Ph) were present in +1 oxidation state [28], corresponding to the binding energy around 85.2 eV in Au$_{4f7/2}$ level. The single XPS peak in Au$_{4f7/2}$ level further confirmed the sole coordination model between the Au(I) ion and the PPh$_2$–ligand. In comparison with free Au(PPh$_3$)Cl, the Au(I) binding energy in the Au–PPh$_2$–PMO(Ph) shifted negatively by 0.3 eV, possibly due to the stronger electron-donating ability of P in the PPh$_2$(CH$_2$CH$_2$) than that in the PPh$_3$, taking into account that $\prod$ conjugated system between P and three phenyl groups could dilute the electron density on the P atom.

Fig. 6 revealed that the Au–PPh$_2$–PMO(Ph) displayed a typical IV type N$_2$ adsorption–desorption isotherm with a H$_1$ hysteresis loop indicative of the mesoporous structure [29]. The low-angle XRD pattern (Fig. 7) showed an intense peak around 2θ = 1.5° indicative of (1 0 0) diffraction and two additional weak peaks at higher 2θ values corresponding to (1 1 0) and (2 0 0) diffractions. These results demonstrated that the Au–PPh$_2$–PMO(Ph) contained ordered 2-dimensional *P6mm* hexagonal mesoporous channels [30], which was further confirmed by TEM images along [1 1 0] and [1 0 0] directions (Fig. 8).
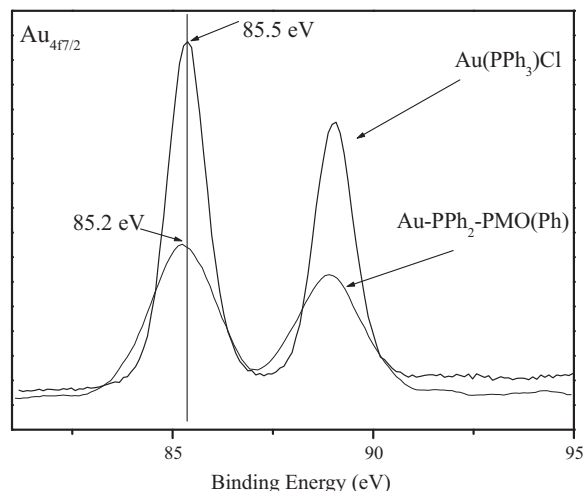
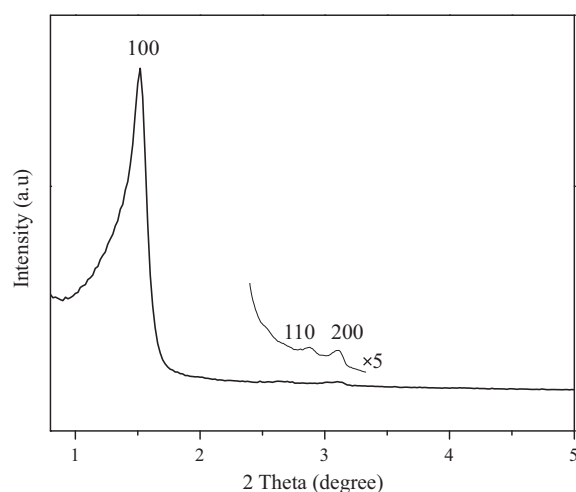

Fig. 7. Low-angle XRD patterns of Au–PPh$_2$–PMO(Ph). The attached is the magnified pattern with 2θ ranging from 1.72° to 3.42°.

The co-condensation between Au[PPh$_2$(CH$_2$)$_2$Si(OCH$_2$CH$_3$)$_3$]$_2$Cl and (CH$_3$CH$_2$O)$_3$SiPhSi(OCH$_2$CH$_3$)$_3$ resulted in two kinds of products. The first kind of product contained Au(I) organometals incorporated into the pore walls of the PMO(Ph) support, as described Scheme 1. The other contained Au(I) organometals terminally bonded to the pore surface (see Scheme 3). Unfortunately, we could not find a direct evidence for distinguishing these two models. Dufaud pointed out that the organometals incorporated in the pore walls had no significant influence on the pore diameter while the organometals terminally bonded to the pore surface might narrow the pore channels [14]. Based on such a conclusion, we prepared the Au–PPh$_2$–PMO(Ph)–G′ by grafting the Au[PPh$_2$(CH$_2$)$_2$Si(OCH$_2$CH$_3$)$_3$]$_2$Cl onto the PMO(Ph) support with all the Au(I) organometals stayed on the pore sur-

Fig. 5. XPS spectra of Au(PPh$_3$)Cl and Au–PPh$_2$–PMO(Ph) samples.
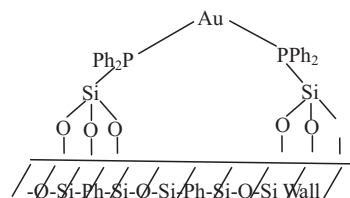
Scheme 3. Structural model of the Au–PPh$_2$–PMO(Ph)–G′ with the Au(I) organometals terminally bonded to the PMO(Ph) pore surface.
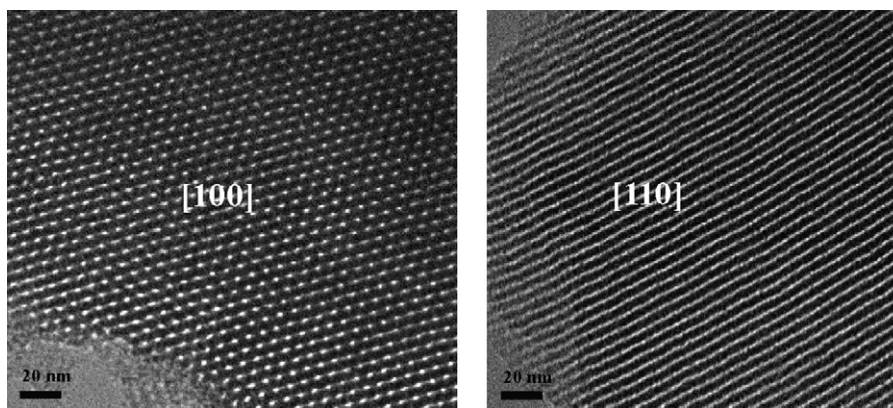
Fig. 8. TEM images of Au–PPh$_2$–PMO(Ph) viewing along [1 1 0] and [1 0 0] directions.

face. Then, we determined pore size distribution of PMO(Ph), Au–PPh$_2$–PMO(Ph) and Au–PPh$_2$–PMO(Ph)–G'. As shown in Fig. 9, the Au–PPh$_2$–PMO(Ph) displayed similar pore diameter to the PMO(Ph) (3.1 nm), while the Au–PPh$_2$–PMO(Ph)–G' displayed smaller pore diameter (2.8 nm) than the PMO(Ph). These results implied that the Au(I) organometals in the Au–PPh$_2$–PMO(Ph) were possibly incorporated into the silica walls rather than grafted onto the pore surface.

A key consideration of the Au–PPh$_2$–PMO(Ph) catalyst is the location of Au(I) species since they should contact with reactant molecules. The bromination test was used to confirm that the vinyl groups in the vinyl-bridged PMO were chemically accessible [16]. To make sure that the Au(I) organometals incorporated into PMO(Ph) pore walls were chemically accessible to the reactant molecules, the Au–PPh$_2$–PMO(Ph) was allowed to react with KMnO$_4$ aqueous solution. Only the Au(I) organometals chemically accessible could be oxidized by KMnO$_4$ while those Au(I) embedded in silica walls could not be oxidized. After complete reaction, the unreacted KMnO$_4$ was titrated by Na$_2$C$_2$O$_4$, from which the amount of Au(I) species was determined. The total Au(I) species were also determined by ICP analysis. The molar ratio between Au(I) species determined by KMnO$_4$ oxidation and by ICP was 93%, suggesting that most of Au(I) active sites in the Au(I)–PPh$_2$–PMO(Ph) were chemically accessible for catalytic reactions.

Some structural parameters including surface area (S_{BET}), pore diameter (D_P) and pore volume (V_P) were summarized in Table 1. Obviously, the Au–PPh$_2$–PMO(Ph) exhibited much higher S_{BET}, D_P and V_P than the Au–PPh$_2$–PMO(Ph)–G with the similar Au load-
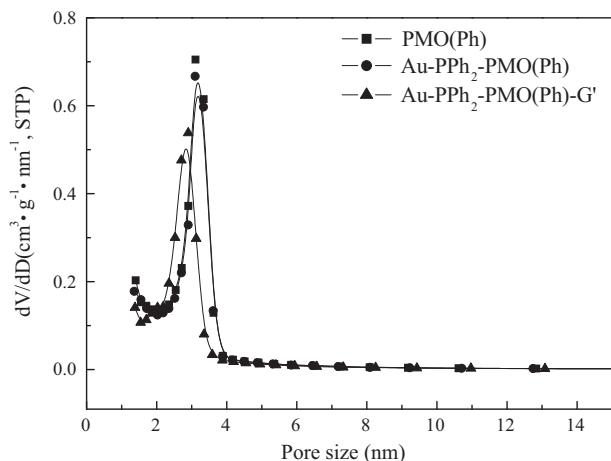
ings. A reasonable explanation was that the Au(I) organometal in the Au–PPh$_2$–PMO(Ph) were embedded into the silica walls. While, the Au(I) organometal in Au–PPh$_2$–PMO(Ph)–G were terminally bonded to the pore surface, which might partially block the mesoporous channels, leading to low S_{BET}, D_P and V_P.

3.2. Catalytic performances

Table 1 summarized the performances of three kinds of Au(I) organometallic catalysts in hydration of phenylacetylene. Besides the unreacted phenylacetylene, only acetophenone was detected by GC–MS analysis, indicating that all these catalysts were almost absolutely selective. The Au–PPh$_2$–PMO(Ph) exhibited much higher activity than the Au–PPh$_2$–PMO(Ph)–G, obviously owing to the higher S_{BET} and larger D_P which facilitated the diffusion and adsorption of reactant molecules. The kinetic studies demonstrated that hydration reaction was first order with respect to alkyne concentration but zero order to water concentration under present conditions, implying the saturated water adsorption while the unsaturated alkyne adsorption on the catalyst. Thus, the enhanced alkyne adsorption could promote the alkyne hydration. To our surprise, the Au–PPh$_2$–PMO(Ph) was even more active than free Au(PPh$_3$)Cl catalyst. One possible reason was the change of coordination model from PPh$_3$–Au–Cl to PPh$_2$–Au–PPh$_2$, which might be more efficiency as the chemical microenvironment of Au(I) active sites for the alkyne hydrogenation. Meanwhile, the presence of phenyl groups in the silica walls might enhance the surface hydrophobolity of the catalyst, which facilitated the alkyne adsorption, especially in aqueous solution. Furthermore, according to the FT-IR spectra of pyridine adsorption (Fig. 10), the PPh$_2$–PMO(Ph), PMO(Ph) and Au–PPh$_2$–PMO(Ph) displayed Lewis acidic sites around 1572, 1594 and 1446 cm^{-1} [31], which might also promote the alkyne hydration [32–34]. Similarly, addition of little amount of H$_2$SO$_4$ during alkyne hydration could also enhance the catalytic activity of Au(PPh$_3$)Cl (see Fig. 11). Although the weaker acidity, the Au(I) organometallic catalyst still exhibited higher activity in the presence of Lewis acid than that in the presence of H$_2$SO$_4$, which could be attributed to the stronger promoting effect of Lewis acid [32–34]. Table 1 also demonstrated that both the PMO(Ph) and the PPh$_2$–PMO(Ph) displayed no significant activities for the phenylacetylene hydration in the presence of H$_2$SO$_4$. Thus, the Au(I) organometals acted as the active center, while the acidic sites acted as the co-catalyst. To make sure whether the heterogeneous Au(I) anchored on the support or homogeneous Au(I) leached from the support was the real catalyst, the following experiments were carried out according to the procedure proposed by Sheldon et al. [35]. After reaction for 3 h with the conversion exceeding 45%, the solid catalyst was filtered out

Fig. 9. Pore size distribution curves of PMO(Ph), Au–PPh$_2$–PMO(Ph) and Au–PPh$_2$–PMO(Ph)–G' samples.

Table 1
Structural parameters and catalytic efficiencies of different catalysts in water-medium hydration of benzyl acetylene.[a]

Sample	Au loading (wt%)	S_{BET} (m²/g)	D_P (nm)	V_P (cm³/g)	Yield (%)
PMO(Ph)	–	968	3.2	0.85	–[b]
PPh$_2$–PMO(Ph)	–	802	3.1	0.63	–[b]
Au(PPh$_3$)Cl	–	–	–	–	24
Au–PPh$_2$–PMO(Ph)–G	0.26	561	2.8	0.40	21 (24)[c]
Au–PPh$_2$–PMO(Ph)	0.22	892	3.1	0.69	91
Used Au–PPh$_2$–PMO(Ph)[d]	0.20	824	3.1	0.61	90

[a] Reaction conditions: a catalyst containing 0.010 mmol of Au, 0.25 mmol phenylacetylene, 0.25 mmol H_2SO_4, 4 mL H_2O, n-decane as an internal standard, temperature = 100 °C, reaction time = 7 h.
[b] Too low to be detected.
[c] The value in the parenthesis was obtained on the Au–PPh$_2$–PMO(Ph)–G catalyst prepared by using Au(tht)Cl instead of Au(PPh$_3$)Cl as gold source.
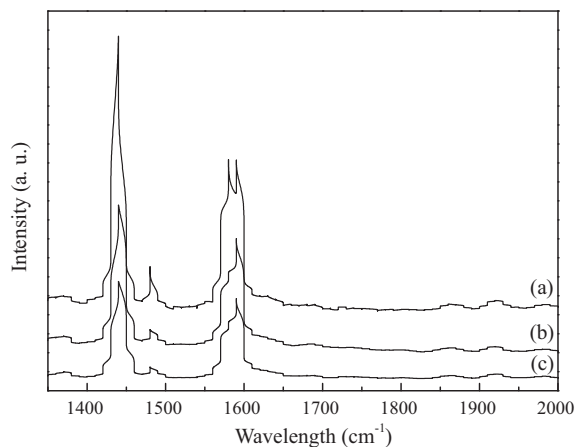[d] After being used repetitively for three times.

Fig. 10. FT-IR spectra of pyridine adsorption on (a) PPh$_2$–PMO(Ph), (b) PMO(Ph), and (c) Au–PPh$_2$–PMO(Ph) at room temperature.

Fig. 11. Effect of the H_2SO_4 concentration on the yield of acetophenone during hydration of benzyl acetylene catalyzed by un-immobilized Au(PPh$_3$)Cl. Reaction conditions: Au(PPh$_3$)Cl catalyst containing 0.010 mmol of Au, 0.25 mmol benzyl acetylene, 4.0 mL H_2O, reaction temperature = 100 °C, reaction time = 7 h.

and the liquid solution was allowed to react for another 7 h under identical reaction conditions. No significant change in either the alkyne conversion or the yield of product was observed, indicating that the active phase was not the Au(I) species leached from the Au–PPh$_2$–PMO(Ph). Therefore, it is reasonable to conclude that the present catalysis was really heterogeneous in nature. Besides the higher activity, the Au–PPh$_2$–PMO(Ph) also showed superiority over the free Au(PPh$_3$)Cl catalyst since it could also be easily recycled and used repetitively. On one hand, the Au(I) organometals embedded in silica walls could effectively inhibit the leaching of Au(I) active sites, which had been confirmed by ICP analysis (see Table 1). On the other hand, the Au(I) organometals embedded in silica walls might also enhance the hydrothermal stability of Au–PPh$_2$–PMO(Ph) [36]. As shown in Fig. 12, both the low-angle XRD pattern and the TEM images demonstrated the preservation
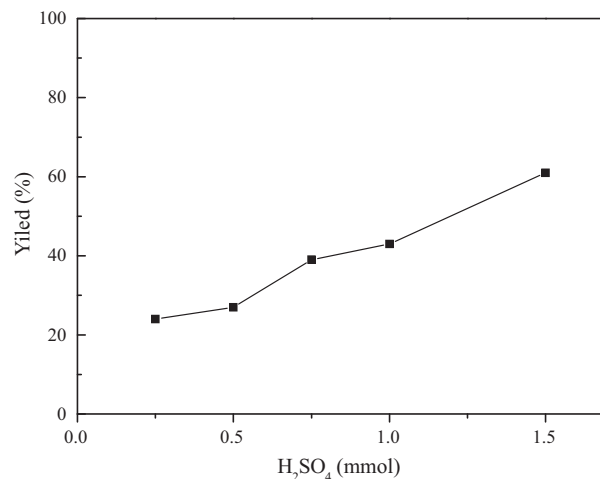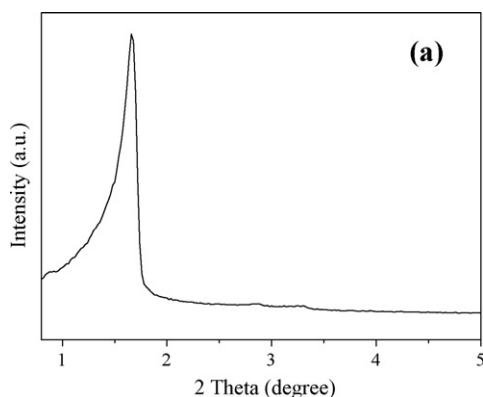
of ordered mesoporous structure in the Au–PPh$_2$–PMO(Ph) catalyst after being used repetitively for 3 times, corresponding to the high S_{BET}, V_P and D_P values (see Table 1).

The catalytic behaviors of the Au–PPh$_2$–PMO(Ph) were also examined in hydration reactions with other terminal alkynes. As shown in Table 2, the Au–PPh$_2$–PMO(Ph) also exhibited higher activity than the Au(PPh$_3$)Cl. It was also found that hydration of terminal aliphatic alkynes and phenylacetylene derivatives containing electron-donating groups exhibited higher activity and yield to target products than those containing electron-withdrawing groups since alkyne hydration was electrophilic in nature [37,38].
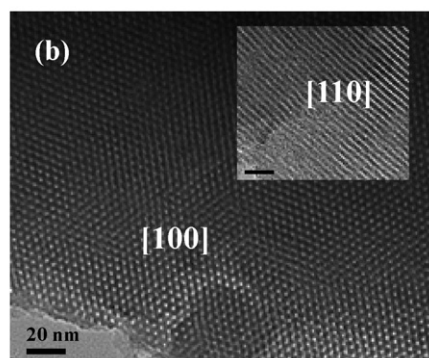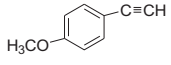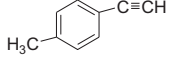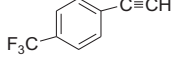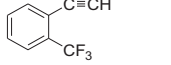

Fig. 12. The low-angle XRD pattern (a) and the TEM images viewing along [1 0 0] and [1 1 0] directions (b) of the Au–PPh$_2$–PMO(Ph) after being used repetitively for 3 times.

Table 2
Catalytic efficiencies of Au–PPh$_2$–PMO(Ph) and Au(PPh$_3$)Cl in hydration reactions of different terminal alkynes.[a]

Alkynes	Conversion (%)	Yield (%)
n-C$_6$H$_{13}$C≡CH	93 (16)	93 (16)
n-C$_8$H$_{17}$C≡CH	92 (13)	92 (13)
H$_3$CO— ⬡ —C≡CH	94 (18)	94 (18)
H$_3$C— ⬡ —C≡CH	89 (16)	89 (16)
F$_3$C— ⬡ —C≡CH	45 (trace)	45 (trace)
⬡ (C≡CH, CF$_3$)	13 (trace)	13 (trace)

[a] Reaction conditions are the same as described in Table 1. The values in the parentheses were obtained by using the Au(PPh$_3$)Cl catalyst.

4. Conclusions

In summary, this work developed a facile approach to synthesize a Au(I) periodic mesoporous organometalsilica catalyst with both the Au(I) organometals and phenyl groups integrally incorporated into the silica walls. During hydration of various terminal alkynes, the Au–PPh$_2$–PMO(Ph) exhibited higher activity than the Au–PPh$_2$–PMO(Ph)–G with the Au(I) organometal terminally bonding to the pore surface of PMO(Ph) support and the free Au(PPh$_3$)Cl since the Au(I) organometals and phenyl groups embedded in silica walls could improve the dispersion and chemical microenvironment of active sites and also enhance the surface hydrophobility without significant pore blockage and damage. The catalyst could be easily recycled and used repetitively owing to the organogold(I) inside silica framework which could enhance the hydrothermal stability and also inhibit the leaching of Au(I) active sites.

Acknowledgements

References

[1] W.A. Herrmann, B. Cornils, Angew. Chem. Int. Ed. 36 (1997) 1048.
[2] Y. Hayashi, Angew. Chem. Int. Ed. 45 (2006) 8103.
[3] R.A. Sheldon, Green Chem. 7 (2005) 2678.
[4] P. Metivier, Fine Chemicals through Heterogeneous Catalysis, Wiley, Weinheim, 2001, p. 161.
[5] H.X. Li, F. Zhang, H. Yin, Y. Wan, Y.F. Lu, Green Chem. 9 (2007) 500.
[6] T. Hirakawa, S. Tanaka, N. Usuki, H. Kanzaki, M. Kishimoto, M. Kitamura, Eur. J. Org. Chem. 6 (2009) 789.
[7] C.J. Cullen, W.R.C. Wootton, A.J. de Mello, J. Appl. Phys. 105 (2009) 102007.
[8] Y. Wan, F. Zhang, Y.F. Lu, H.X. Li, J. Mol. Catal. A 267 (2006) 165.
[9] H.X. Li, F. Zhang, Y. Wan, Y.F. Lu, J. Phys. Chem. B 110 (2006) 22942.
[10] H.X. Li, M.W. Xiong, F. Zhang, J.L. Huang, W. Chai, J. Phys. Chem. C 112 (2008) 6366.
[11] W.H. Zhang, X.B. Lu, J.H. Xiu, Adv. Funct. Mater. 14 (2004) 544.
[12] X.S. Yang, F.X. Zhu, J.L. Huang, F. Zhang, H.X. Li, Chem. Mater. 21 (2009) 4925.
[13] J.L. Huang, F.X. Zhu, W.H. He, F. Zhang, W. Wang, H.X. Li, J. Am. Chem. Soc. 132 (2010) 1492.
[14] V. Dufaud, F. Beauchesne, L. Bonneviot, Angew. Chem. Int. Ed. 44 (2005) 3475.
[15] S. Inagaki, S. Guan, Y. Fukushima, O. Terasaki, J. Am. Chem. Soc. 121 (1999) 9611.
[16] T. Asefa, M.J. Maclachlan, N. Coombs, G.A. Ozin, Nature 402 (1999) 867.
[17] K.J. Shea, D.A. Loy, Chem. Mater. 13 (2001) 3306.
[18] F. Hoffmann, M. Cornelius, J. Morell, M. Froba, Angew. Chem. Int. Ed. 45 (2006) 3216.
[19] T. Asefa, M. Kruk, N. Coombs, H. Grondey, M.J. MacLachlan, M. Jaroniec, G.A. Ozin, J. Am. Chem. Soc. 125 (2003) 11662.
[20] O. Krcher, R.A. Kppel, M. Frba, J. Catal. 178 (1998) 284.
[21] Q.Y. Hu, J.E. Hampsey, N. Jiang, C.J. Li, Y.F. Lu, Chem. Mater. 17 (2005) 1561.
[22] H. Huang, R. Yang, D. Chinn, C.J. Munson, Ind. Eng. Chem. Res. 42 (2003) 2427.
[23] M. Burleigh, A. Michael, M. Markowitz, S. Spector, B. Gaber, J. Phys. Chem. B 105 (2001) 9935.
[24] S. Inagaki, S. Guan, T. Ohsuna, O. Terasaki, Nature 416 (2002) 304.
[25] P.F.W. Simon, R. Ulrich, H.W. Spiess, U. Wiesner, Chem. Mater. 13 (2001) 3464.
[26] T. Posset, F. Rominger, J. Blumel, Chem. Mater. 17 (2005) 586.
[27] Q. Yang, J. Liu, J. Yang, M.P. Kapoor, S. Inagaki, C. Li, J. Catal. 228 (2004) 265.
[28] J.F. Moulder, W.F. Stickle, P.E. Sobol, K.D. Bomben, Handbook of X-ray Photoelectron Spectroscopy, A Reference Book of Standard Spectra for Identification and Interpretation of XPS Data, Perkin-Elmer Corporation, Physical Electronics Division, USA, 1992, p. 183.
[29] D.Y. Zhao, Q. Huo, J. Feng, B.F. Chmelka, G.D. Stucky, J. Am. Chem. Soc. 120 (1998) 6024.
[30] J.R. Matos, M. Kruk, L.P. Mercuri, N. Coombs, G.A. Ozin, T. Kamiyama, J. Terasaki, Chem. Mater. 14 (2002) 1903.
[31] G. Busca, Phys. Chem. Chem. Phys. 1 (1999) 723.
[32] M. Impéror-Clerc, P. Davidson, A. Davidson, J. Am. Chem. Soc. 125 (2003) 11925.
[33] X. Wu, D. Bezier, C. Darcel, Adv. Synth. Catal. 351 (2009) 367.
[34] J.H. Teles, S. Brode, M. Chabanas, Angew. Chem. Int. Ed. 37 (1998) 1415.
[35] R.A. Sheldon, Green Chem. 7 (2005) 267.
[36] A.D. Allen, Y. Chiang, A. Kresge, T.T. Tidiwell, J. Org. Chem. 47 (1982) 775.
[37] R. Casado, M. Contel, M. Laguna, P. Romero, S. Sanz, J. Am. Chem. Soc. 125 (2003) 11925.
[38] J.E. Herrera, J. Kwak, J.Z. Hu, Y. Wang, C.H.F. Peden, J. Macht, E. Iglesia, J. Catal. 239 (2006) 200.